Synthesis of $Co_2P_4O_{12}$ porous structure and non-isothermal decomposition kinetics of $Co(H_2PO_4)_2•2H_2O$ precursor in air atmospheres

Banjong Boonchom

King Mongkut's Institute of Technology Ladkrabang Chumphon Campus, 17/1 M. 6 Pha thiew District, Chumphon, 86160, Thailand

The thermal decomposition of $Co(H_2PO_4)_2•2H_2O$ was studied in air atmosphere using TG-DTG-DTA. TG-DTG-DTA curves show that the decomposition occurs in three steps, which are dehydration processes. The thermal stability of the $Co(H_2PO_4)_2•2H_2O$ was studied by means of the non-isothermal kinetic (Kissinger method). The specificity of thermal decomposition was characterized by identification of the bonds to be selectively activated due to energy absorption at vibrational level, which was assigned by comparison the calculated wavenumbers with the observed wavenumbers in FTIR spectra. These results were used to identify the molecules or ions that were eliminated in each thermal transition step. The $Co(H_2PO_4)_2•2H_2O$ and its thermal transformation products were characterized by scanning electron microscopy (SEM), X-ray powder diffraction (XRD), Fourier transform infrared (FTIR) and UV-vis near IR techniques. The final decomposition product $Co_2P_4O_{12}$ appears micropores and macropores on the surface of the particle, which is important for specific applications.

Keywords: $Co(H_2PO_4)_2•2H_2O$, Cobalt Cyclotetraphosphate, Porous Structure, Non-Isothermal kinetics

(Received January 12, 2009; accepted March 23, 2009)

1. Introduction

The acid phosphates of some bivalent metals have been reported to be the important inorganic compounds in during the last decades [1-5]. They are generally known to posses optical, electric and magnetic properties of practical importance, which are determined by the presence of very strong hydrogen bonds in their crystal lattices [6]. In particular, manganese, iron, cobalt, nickel and zinc dihydrogen phosphates are components of corrosion-proof compositions [7]. Calcium, manganese and iron dihydrogen phosphates are valuable phosphorus and micronutrient fertilizer due to their solubility in soil [7]. The dihydrate belongs to the well-known series of isostructural crystallohydrates $M(H_2PO_4)_2•2H_2O$ (M= Mg, Mn, Co, Ni, Fe, Zn), which have similar X-ray diffraction patterns and close unit cell parameters (they crystallize in monoclinic space group $P2_1/n$ with Z = 2) [9-12]. The $M(H_2PO_4)_2•2H_2O$ was synthesized from metal(II) carbonate and phosphoric acid at low temperature (40-80 ^oC) with long time periods (> 8 h) [6, 10]. So far, only the crystal structure and thermal analysis of $M(H_2PO_4)_2•2H_2O$ have been reported [6, 9, 13-14]. Most recently, Koleva et al. [10] reported the crystal structure and magnetic property of $M(H_2PO_4)_2•2H_2O$ (M=Mg, Mn, Fe, Co, Ni, Zn, Cd). When calcined, dihydrogenphosphates yield cyclotetraphosphates, which are used as pigments, catalysts, and luminophore-supporting matrices [15-18]. Therefore, thermal treatments of these dihydrogen phosphate hydrates have a great synthetic potential, which relates to the hydrate in the conventional

crystal form. The presence of the water molecules influences the intermolecular interactions (affecting the internal energy and enthalpy) as well as the crystalline disorder (entropy) and, hence, influences the free energy, thermodynamic activity, solubility, stability, electrochemical and catalytic activity [19-20]. To control the state of hydration of the active ingredient, it is, therefore, important and necessary to understand the kinetics and mechanisms of decomposition and dehydration processes under the appropriate conditions. In many methods of kinetics estimation, isoconversional method is recommended as trustworthy way of obtaining reliable and consistent kinetic information [21-21]. It is a 'model-free method', which involves measuring the temperatures corresponding to fixed values of the extent of conversion (α) from experiments at different heating rates (β). The results obtained on these bases can be directly applied in materials science for the preparation of various metals and alloys, ceramics, glasses, enamels, glazes, polymer and composite materials.
In this respect, the formation of $Co_2P_4O_{12}$ porous structure from $Co(H_2PO_4)_2•2H_2O$ was followed using differential thermal analysis-thermogravimetry (TG-DTG/DTA), X-ray powder diffraction (XRD), scanning electron microscopy (SEM) Fourier transform-infrared (FT-IR) and UV-vis-near-IR techniques. Thermal stability of $Co(H_2PO_4)_2•2H_2O$ was studied by means of the non-isothermal kinetics (Kissinger method) [23], in which a correlation between the temperature, activation energy and the wavenumbers assigned to the bond responsible for the thermal decomposition of this compound are suggested for the first time.

2. Experimental procedures

2.1 Preparation

The compound $Co(H_2PO_4)_2•2H_2O$ was prepared by solution precipitation method using cobalt carbonate ($CoCO_3$, 99.99%, Merck,) and phosphoric acid (86.4%w/w H_3PO_4, Merck) as starting materials. About 1.2 g of $CoCO_3$ were dissolved in 70 % H_3PO_4 (86.4 %w/w H_3PO_4 dissolved in DI water) with continuous stirring at 40 ^oC on a hot plate. The resulting solution was stirred until CO_2(g) was completely evolved (15-30 min) and the precipitates were obtained. The nearly dry sample was obtained and then 10 mL of acetone was added to allow highly crystalline product to be developed. The prepared solid was filtered by suction pump, washed with acetone and dried in air.

2.1 Characterization methods

`The water content was analyzed by TG data. Thermal properties of $Co(H_2PO_4)_2•2H_2O$ was investigated on a TG- DTG-DTA Pyris Diamond Perkin-Elmer Instruments. The experiments were performed in static air, at the heating rates of 5, 10, 15, and 20 K min^{-1} over the temperature range from 303 to 873 K and the O_2 flow rate of 100 mL min^{-1}. The sample mass of about 6.0 -10.0 mg was filled into alumina crucible without pressing. The thermogram of a sample was recorded in an open alumina pan using α-Al_2O_3 as the reference material. The synthesized $Co(H_2PO_4)_2•2H_2O$ was calcined in a box-furnace at 773 K in air and the thermal transformation products were further investigated. The structure and crystalline size of the prepared $Co(H_2PO_4)_2•2H_2O$ and its thermal transformation products were studied by X-ray powder diffraction using X-ray diffractometer (Phillips PW3040, The Netherland) with Cu Kα radiation (λ = 0.1546 nm). The Scherrer method was used to evaluate the crystalline size (i.e. $D = K\lambda/\beta\cos\theta$, where λ is the wavelength of X-ray radiation, K is a constant taken as 0.89, θ is the diffraction angle and β is the full width at half maximum (FWHM)) [24]. The morphologies of the selected resulting samples were examined by scanning Eelectron microscope using LEO SEM VP1450 after gold coating. The room temperature FTIR spectra were recorded in the range of 4000-370 cm^{-1} with 8 scans on

a Perkin-Elmer Spectrum GX FT-IR/FT-Raman spectrometer with the resolution of 4 cm^{-1} using KBr pellets (spectroscopy grade, Merck).

3. Results and discussion

3.1 Thermal Stability of $Co(H_2PO_4)_2•2H_2O$

The TG-DTG-DTA curves of $Co(H_2PO_4)_2•2H_2O$ are shown in Figure 1. The TG curve of $Co(H_2PO_4)_2•2H_2O$ show the weight loss in the range of 353-873 K. The eliminations of water were observed in three areas: 353-473, 473-573 and 573-703 K.

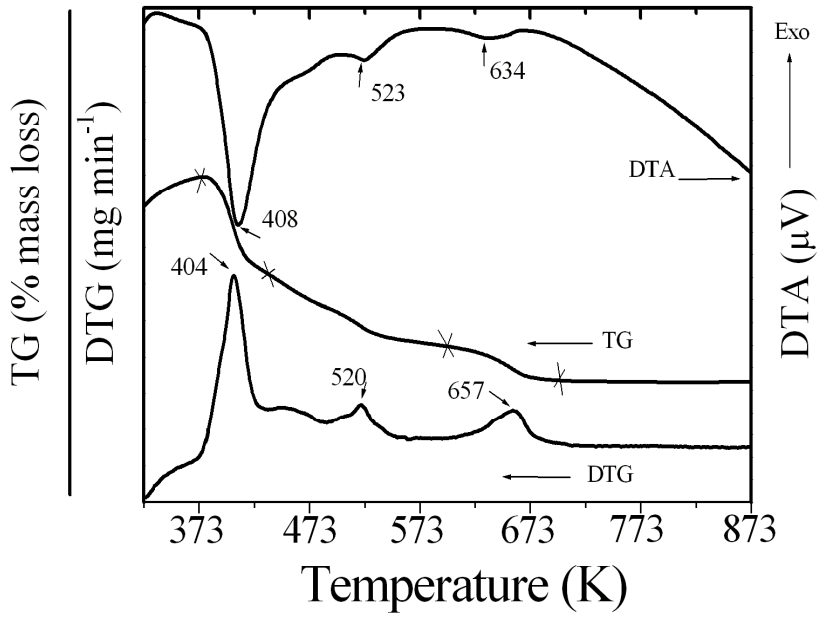

Figure 1 TG-DTG-DTA curves of $Co(H_2PO_4)_2•2H_2O$ at heating rate of 10 K min^{-1} in air

The corresponding observed weight losses are 10.70, 7.27 and 4.76% by mass, which correspond to 1.72, 1.17, and 0.76 mol of water, respectively. Three endothermic effects on DTA curves are observed at 408, 523 and 634 K, which correspond to DTG peaks at 404, 520 and 657 K, respectively. The thermal decomposition of $Co(H_2PO_4)_2•2H_2O$ is a complex process, which involve the dehydration of the coordinated water molecules (~2 mol H_2O) in the first step and an intramolecular dehydration of the protonated phosphate groups (~2 mol H_2O) in last two steps, the process could be formally presented as:

$$Co(H_2PO_4)_2•2H_2O \longrightarrow Co(H_2PO_4)_2 + \sim 2H_2O \quad (1)$$

$$Co(H_2PO_4)_2 \longrightarrow CoH_2P_2O_7 + \sim H_2O \quad (2)$$

$$CoH_2P_2O_7 \longrightarrow 1/2Co_2P_4O_{12} + \sim H_2O \quad (3)$$

A large number of intermediate compounds, such as acid polyphosphate $Co(H_2PO_4)_2$, acid condensed phosphate $CoH_2P_2O_7$ and mixtures of intermediate of both have been registered. Cobalt cyclotetraphosphate $Co_2P_4O_{12}$ was found to be the products of the thermal decomposition in the range of 673-873 K as revealed by the TG curve. The total mass loss is 22.73 % (3.64 mol H_2O), which are close to theoretical value (24.92 % (4 mol H_2O) and these results are also in agreement with those reported in literatures [6, 9]. In order to gain the

complete dehydration of synthesized $Co(H_2PO_4)_2 \bullet 2H_2O$, the sample of $Co(H_2PO_4)_2 \bullet 2H_2O$ was heated in the furnace at 773 K for
3 h and the dehydrated product was found to be cobalt cyclotetraphosphate ($Co_2P_4O_{12}$).

3.2 X-ray powder diffraction

The XRD patterns of $Co(H_2PO_4)_2 \bullet 2H_2O$ and its decomposition product $Co_2P_4O_{12}$ are shown in Figure 2.

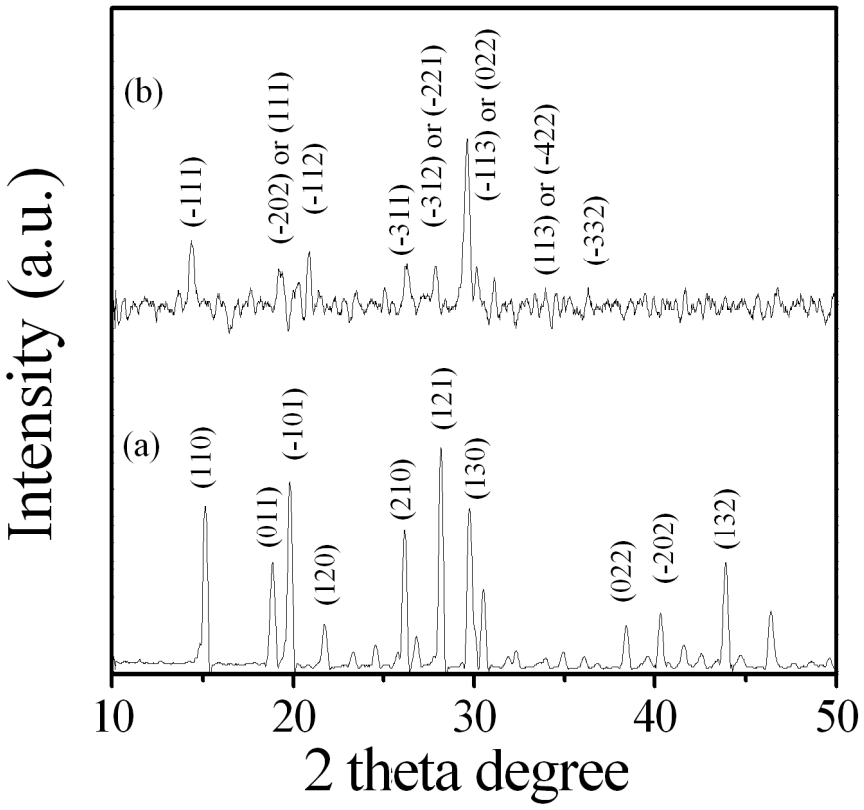

Figure 2 The XRD patterns of $Co(H_2PO_4)_2$•$2H_2O$ (a) and its dehydration product $Co_2P_4O_{12}$ (b).

All detectable peaks of the $Co(H_2PO_4)_2 \bullet 2H_2O$ and $Co_2P_4O_{12}$ are indexed as $Co(H_2PO_4)_2 \bullet 2H_2O$ and $Co_2P_4O_{12}$ structures, which are identified using the standard data of PDF no. 390698 and PDF no. 842208, respectively. These results indicated that the two crystal structures are in monoclinic system with space group $P2_1/n$ (Z = 2) for $Co(H_2PO_4)_2 \bullet 2H_2O$ and C2/c (Z = 4) for $Co_2P_4O_{12}$. The average crystallite sizes and lattice parameters of $Co(H_2PO_4)_2 \bullet 2H_2O$ and $Co_2P_4O_{12}$ were calculated from X-ray spectra and are tabulated in Table 1.

Table 1 Kinetic parameter and band assignments [10, 12, 30]

Step	Temperature (K) in four heating rate (β)				Average T_p	E_a/ kJmol^{-1}	r^2	q	nω/ cm^{-1}	Band assignment
	5	10	15	20						
1	393.15	398.15	401.15	403.45	398.98	171.43±1.63	0.99991	6	1663	ν_2 (H_2O)
								12	3327	ν_1 (H_2O)
								13	3604	ν_3 (H_2O)
2	505.36	512.39	516.97	520.03	513.69	197.24±2.52	0.99984	2	714	γ_{OH} ($H_2PO_4^-$)
								3	1071	ν (PO_2)
								5	1785	Band C ($H_2PO_4^-$
								7	2499	Band B ($H_2PO_4^-$)
								9	3213	Band A ($H_2PO_4^-$)
3	621.15	635.99	647.65	654.15	639.74	129.24±5.20	0.99839	1	444	δ (O_2PO_2)
								2	889	ν ($PO_2(H_2)$)
								4	1778	Band C ($H_2PO_4^-$

The lattice parameters of $Co(H_2PO_4)_2 \cdot 2H_2O$ and $Co_2P_4O_{12}$ are comparable to those of the standard data of PDF no. 390698 and PDF no. 842208, respectively.

3.3 Vibrational spectroscopy

The FT-IR spectra of $Co(H_2PO_4)_2 \cdot 2H_2O$ and $Co_2P_4O_{12}$ are shown in Figure 3, which are very similar to those of $M(H_2PO_4)_2 \cdot 2H_2O$ and MP_4O_{12} (where M = Mn, Co, Ni) [6, 10-12] Vibrational bands are identified in relation to the crystal structure in terms of the fundamental vibrating units namely $H_2PO_4^-$ and H_2O for $Co(H_2PO_4)_2 \cdot 2H_2O$ and $[P_4O_{12}]^{4-}$ ion for $Co_2P_4O_{12}$, which are assigned according to the literatures [11-12]. Vibrational bands of $H_2PO_4^-$ ion are observed in the regions of 300-500, 700-900, 1160–900, 840-930, 1000-1200 and 2400-3300 cm^{-1}. These bands are assigned to the δ(O_2PO_2), γ(POH), δ(POH), ν($PO_2(H_2)$), ν(PO_2) and ν(OH of H_2O molecules and $H_2PO_4^-$ ions) and , respectively. The observed bands in 1600-1700 cm^{-1} and 3000-3500 cm^{-1} region are attributed to the water bending/C band and stretching vibrations/A band, respectively. Vibrational bands of $[P_4O_{12}]^{4-}$ ion are observed in the ranges of 1350-1220, 1150-1100, 1080-950, and 780-400 cm^{-1}. These bands can be assigned to $\nu_{as}OPO^-$, ν_sOPO^-, $\nu_{as}POP$, and ν_sPOP vibrations, respectively [25].

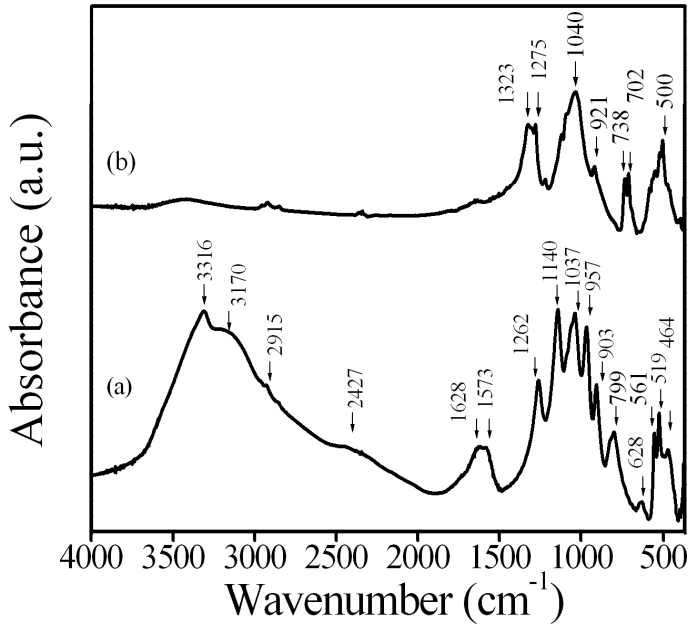

Figure 3 FTIR spectra of $Co(H_2PO_4)_2.2H_2O$ (a) and its dehydration product $Co_2P_4O_{12}$ (b).

The observation of a strong ν_sPOP band is known to be the most striking feature of cyclotetraphosphate spectra, along with the presence of the $\nu_{as}OPO^-$ band. The FTIR results are in consistent with the XRD data (Figure 2).

3.4 Scanning electron microscopy

The SEM micrographs of the synthetic $Co(H_2PO_4)_2$•$2H_2O$ and its decomposition product $Co_2P_4O_{12}$ show non-uniform morphological features (Figure 4).

The SEM micrograph of $Co(H_2PO_4)_2$•$2H_2O$ consists of non-uniform spherical grains, which contains microparticles having a distribution of small particles (2-8 μm) and large particles (>10-100 μm). The SEM micrograph of $Co_2P_4O_{12}$ shows a porous structure and agglomeration, which appear micropores (100–400 nm) and macropores (500-2000 nm) are due to the process of thermal decomposition. The different porous sizes of $Co_2P_4O_{12}$ primarily cause by the process of dehydration, which relate to an intramolecular dehydration of the protonated dihydrogen phosphate groups. The results may be potentially useful for catalyst application because of the catalytic activity of $Co_2P_4O_{12}$ varies significantly with the method of precipitation, thermal treatment and porous structure on the surface [26].

Figure 4a

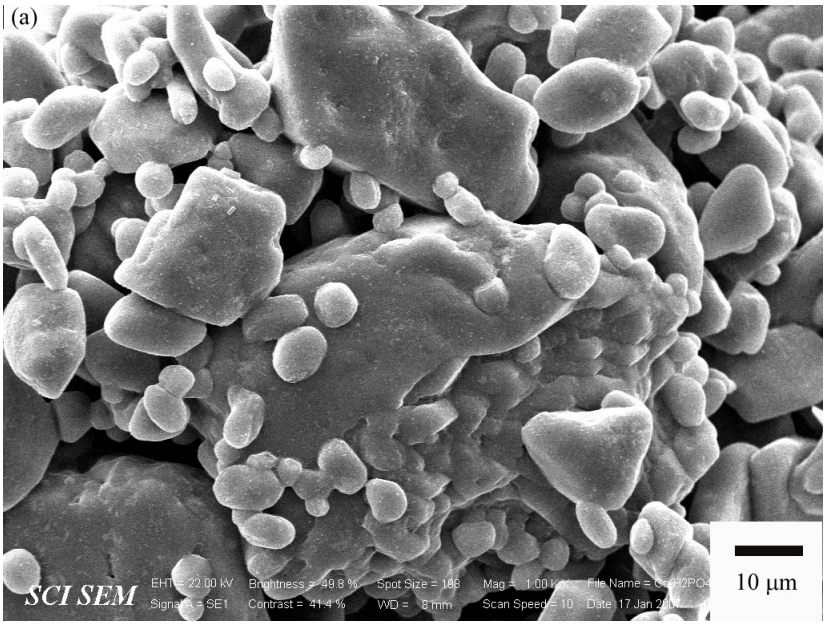

Figure 4b

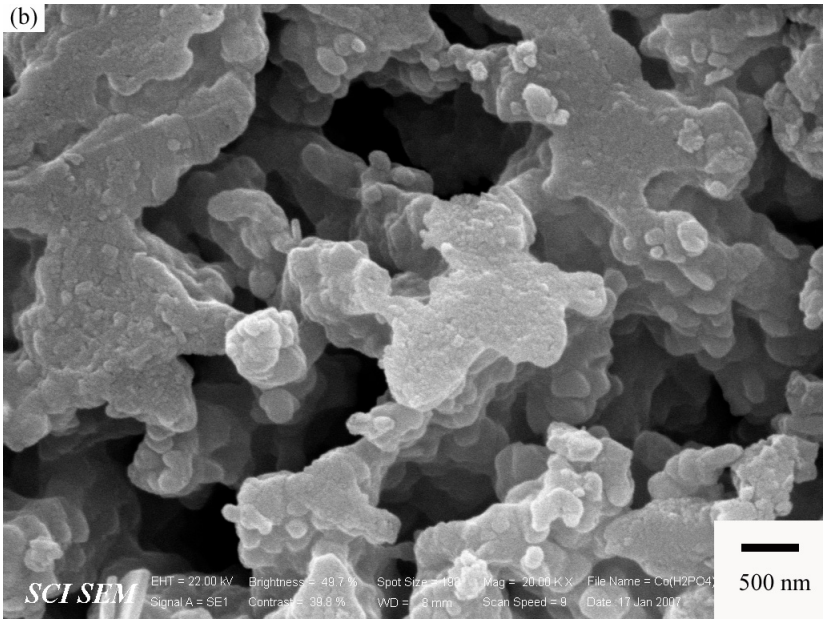

Figure 4 SEM micrographs of $Co(H_2PO_4)_2.2H_2O$ (a) and its dehydration product $Co_2P_4O_{12}$ (b).

3.5 UV-vis near IR spectroscopy

The UV–Vis near IR absorption spectrum of $Co(H_2PO_4)_2$•$2H_2O$ is shown in Figure 5a. The UV-Vis spectrum of $Co(H_2PO_4)_2$•$2H_2O$ shows dominant feature of Co^{2+} in octahedral sites is too weak to be observed as it involves spin- forbidden transitions. The absorption bands of $Co(H_2PO_4)_2$•$2H_2O$ powder are observed and labeled as 1, 2, 3 and 4 around wavelengths of 472, 563, 696 and 1200-1400 nm, respectively.

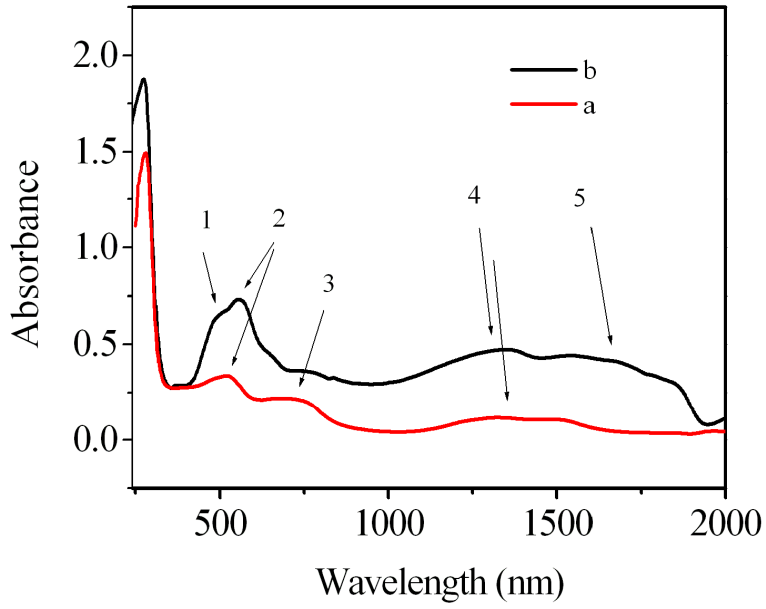

Figure 5 UV-Vis-near IR spectra of $Co(H_2PO_4)_2.2H_2O$ (a) and its dehydration product $Co_2P_4O_{12}$ (b).

The results indicate that Co^{2+} in a distorted octahedral site in the structure (Jahn-Teller effect; it was extensively discussed [27]). The band around 255 nm is too strong to be d-d transitions, lying in the UV region; it is assigned to a charge-transfer band. In six-coordinate, high spin Co(II) complexes a band near 1440–1000 nm can be assigned to the $^4T_{1g} \rightarrow {}^4T_{2g}$ transition. In addition, a multiple structured band, assigned to $^4T_{1g} \rightarrow {}^4T_{1g}(P)$, is seen in the visible region near 500 nm , which is split into two components (472 and 563 nm). The weak absorption at 696 nm is due to the $^4T_{1g} \rightarrow {}^4A_{2g}$ transition. Figure 5b shows the UV-vis spectra of $Co_2P_4O_{12}$ compound. Co(II) in octahedral sites are present in these structures [28]. The spectral feature of octahedral site in $Co_2P_4O_{12}$ appear at 513 (1), 563 (2), 753 (3) and 1328 (4) nm, (peak numbers are given in parentheses). These absorption bands are assigned to $^4T_1g \rightarrow {}^4T_{2g}(P)$ transition for a multiple structure band (513 and 563 nm) while the observed absorption bands at ca. 753 and 1328 nm are attributed to the $^4T_{1g} \rightarrow {}^4A_{2g}$ and $^4T_1g \rightarrow {}^4T_{2g}$ transitions, respectively [29].

3.5 Kinetics studies

The aim of the kinetic studies of TA data is to find the most probable kinetics model which gives the description of the studied decomposition process and allows the calculation of liable values for the kinetic triplet (E_a, A and reaction model). To evaluate the activation energies for the thermal decomposition of $Co(H_2PO_4)_2$ •$2H_2O$, DTG technique was performed in static air, at heating rates of 5, 10, 15, and 20 K min^{-1} over the temperature range from 303

to 773 K and the O_2 flow rate of 100 mL min^{-1}. The activation energies for the thermal transformation steps were calculated from three endothermic DTG peaks (Figure 6).

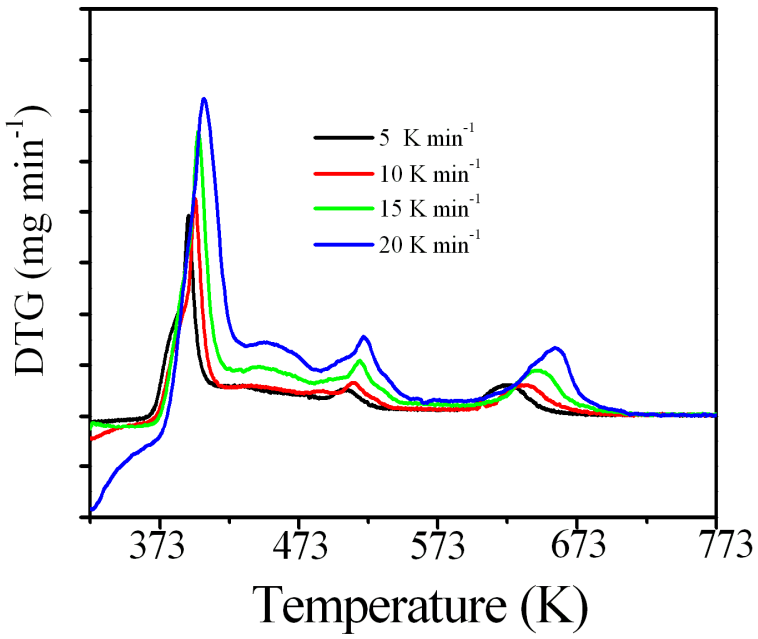

Figure 6 DTG curves of $Co(H_2PO_4)_2.2H_2O$ at four different heating rates in air (5, 10, 15 and 20 K min^{-1}).

Several non-isothermal techniques have been proposed which are quicker and less sensitive to previous and next transformations. In addition, they can provide the more accurate activation energy and crystal growth mode. Non-isothermal data are typically interpreted using Kissinger equation [23],

$$\ln\left(\frac{\beta}{T^2}\right) = -\frac{E_a}{RT_p} + \text{const.} \quad (4)$$

Here, β is the DTG scan rate (K mim^{-1}), E_a is the activation energy for the phase transformation (kJ mol^{-1}), T_p is the phase transformation peak temperature (K) and R is the gas constant (8.314 $kJmol^{-1}K^{-1}$). Figure 7 shows the Kissinger plots of the three decomposition steps of the prepared $Co(H_2PO_4)_2 \bullet 2H_2O$ sample. From the slopes of the curves, the activation energy values of the prepared $Co(H_2PO_4)_2 \bullet 2H_2O$ sample in three steps were calculated to be 171.43 ± 1.63, 197.24 ± 2.52 and 129.24 ± 5.20 $kJmol^{-1}$, respectively (Table 2).

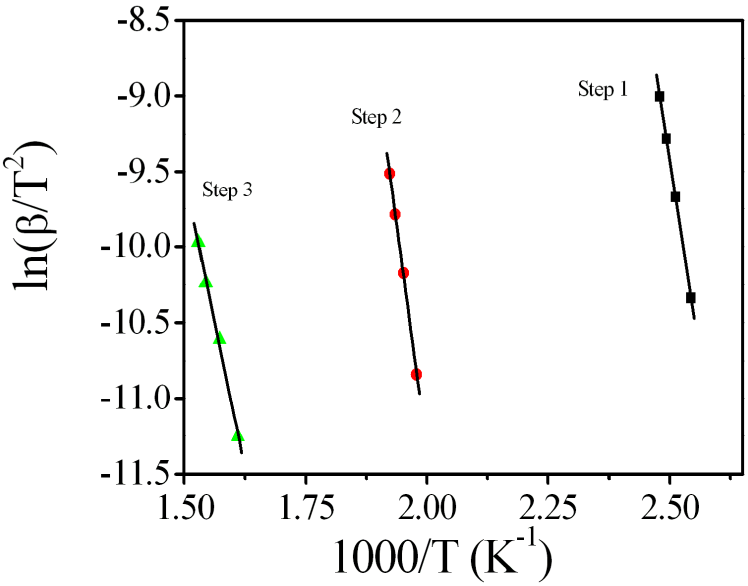

Figure 7 KAS analysis of three decomposition steps of $Co(H_2PO_4)_2.2H_2O$ at four different heating rates in air (5, 10, 15 and 20 K min^{-1}).

The water in crystalline hydrate may be considered either as water of crystallization (crystal water) or as co-ordinated water. The activation energy for the release of the water of crystallization lie in the range of 50–120 kJ mol^{-1}, while the values for coordinately bounded one are higher than this range [21]. In addition, the water eliminated at 423 K and below can be considered as water of crystallization, whereas water eliminated at 473 K and above indicates its co-ordination by the metal atom [19-22]. The calculated activation energies from Kissinger method for the three dehydration reactions suggest that the water molecules are the water of crystallization and co-ordinately water for all decomposition steps. These activation energies are related to the vibration frequencies and are the indication of the energy of the breaking bond of intermediate species. The second step exhibits higher activation energy in comparison with other steps, and this is understandable because this step corresponds to a true P-OH bond breaking, in connection with polycondensation reaction [12]. The lowest activation energy in the last step indicates that non stability of the intermediate compounds ($Co(H_2PO_4)_2$, $CoH_2P_2O_7$ and mixtures of both intermediates) before transform to $Co_2P_4O_{12}$. This result is in consistent with TG-DTG-DTA data as shown in Eq.2-3.

The specificity of the thermal decomposition was characterized by identification of the bonds to be selectively activated due to energy absorption at vibrational level [30]. These bonds were assigned by comparing the calculated wavenumbers with the observed wavenumbers in the IR spectra. The specificity of decomposition under non-isothermal conditions is due to a selective vibrational energy accumulation on a certain bond. This breaking bond is assimilated with a Morse oscillators [30] coupled non-linear [31] with the harmonic oscillators of the thermic field. Following a theoretical treatment developed by Vlase et al.[32], the relation between the isokinetic temperature (T_i) and the wavenumber of the activated bond is given as follows:

$$\omega_{cal} = \frac{k_b}{hc} T_i = 0.695 T_i \quad (5)$$

where k_b and h are respectively the Boltzmann and Planck constants, and c the light velocity. Because the breaking bond has an unharmonic behavior, the specific activation is possible due to more than one quanta, or by a higher harmonic. Here, ω_{cal} is calucated by Eq.(5), which is assigned the spectroscopic number for the bond supposed to break. ω_{sp} is the

frequency bands of vibrational modes and is calculated by $\omega_{sp} = q\omega_{calc}$, $q \in N$=1,2,3,…, (quanta number). Additionally, the ω_{cal} values with the ω_{sp} values determined from the DTG, together with the assignments of the corresponding oscillations are compared. In this paper we suggested the maximum peak temperature T_p in DTG curve for the calculated wavenumbes (ω_{sp}) according to Eq. (6). In order to corroborate the calculated data with the spectroscopic ones, we drew up the FT-IR spectra of the studied compound (Figure 6). Table 2 shows the comparison of the ω_{calc} values with the ω_{sp} values determined from this compound, together with the assignments of the corresponding vibrational modes in the literature [30-31].

Table 2 Average crystallite sizes and lattice parameters of $Co(H_2PO_4)_2$•$2H_2O$ and $Co_2P_4O_{12}$ calculated from XRD data

Compound	**Method**	**a/ Å**	**b/ Å**	**c/ Å**	**β/ o**	**Average crystallite sizes/nm**
$Co(H_2PO_4)_2$•$2H_2O$	PDF no.390698	7.27	9.88	5.33	94.86	
	This work	7.21(3)	9.91(1)	5.29(5)	94.88(6)	26± 2
$Co_2P_4O_{12}$	PDF no.842208	11.8	8.28	9.92	118.72	
	This work	11.83(8)	8.22(6)	9.94(0)	118.51(1)	40 ± 10

This thermal decomposition kinetics studied three mass loss steps, which correspond to the loss of co-ordinated water (the first step), followed by a continuous intermolecular polycondensation and elimination of water (two last steps). The studied compound exhibited a very good agreement between the calculated wavenumbers from average T_p (DTG) and the observed wavenumbers from IR spectra for the bonds suggested being broken. Therefore, the use of T_p (DTG) will be an alternative method for the calculated wave numbers for identification in each thermal transition step of interesting materials.

4. Conclusions

The $Co(H_2PO_4)_2 \cdot 2H_2O$ was decomposed three steps ,which relate the dehydration reaction and its decomposition product is coblat cyclotetraphosphate ($Co_2P_4O_{12}$). The XRD, FTIR and UV-vis-near-IR results confirmed the formation of $Co(H_2PO_4)_2 \cdot 2H_2O$ and $Co_2P_4O_{12}$ compounds. Thermal kinetic study results indicate the activation energies, which relate to vibrational frequencies of breaking bond of thermal transformation of $Co(H_2PO_4)_2$ •$2H_2O$. The thermal behaviors, morphologies and particle sizes of $Co(H_2PO_4)_2$•$2H_2O$ and its thermal transformation product ($Co_2P_4O_{12}$) show interesting of some physical and chemical properties. These materials may be useful for many potential application including catalytic, ceramic dye pigment and magnetic materials etc.

Acknowledgements

The author thanks the Chemistry and Physics Departments, Khon Kaen University for providing research facilities. This work is financially supported by King Mongkut's Institute of Technology Ladkrabang (KMITL), Ministry of Education, Thailand.

References

[1] A. Jouini, J.C. Gâcon, M. Ferid, M. Trabelsi-Ayadi, Opt. Mater. 24, 175 (2003).
[2] T. Kitsugi, T. Yamamuro, T. Nakamura, M. Oka, Biomaterials. 16, 1101 (1995).
[3] B. Jian-Jiang, K. Dong-Wan, H. Kug Sun, J. Eur. Ceram. Soc. 23, 2589 (2003).
[4] J. R. Martinelli, F. F. Sene, L. Gomes, J. Non-Cryst. Solids. 263, 299 (2000).
[5] P. Carmen, P. Josefina, S.P. Regino, R.V. Caridad, S. Natalia, Chem. Mater. 15, 3347 (2003).
[6] V. Koleva, D. Mehandjiev, Mater. Res. Bull. 41, 3, 469 (2006).
[7] M. Trojan, D. Brandova and M. Kuchler, Proc State Conf. on Industrial Fertilizers, Ustinad Labem, , DT CSVTS p. 111 (1985).
[8] M. Bagieu-Beucher, M. Gondrand, M. Perroux, J. Solid State Chem. 19, 353 (1976).
[9] Th. R. Hinsch, W. Guse , H. Saalfeld. J. Cryst. Growth. 79, 205 (1986).
[10] V. Koleva, H. Effenberger, J. Solid State Chem. 180 (2007)956.
[11] B. Boonchom, S. Youngme, S. Maensiri, C. Danvirutai. J. Alloys Compd. xxx (2006) xxx. (doi:10.1016/j.jallcom.2006.12.064).
[12] B. Boonchom, C. Danvirutai, S. Maensiri, Mater. Chem. Phys. xxx (2008) xxx. (doi:10.1016/j.matchemphys.2007.12.018).
[13] H. Effenberger, Acta Cryst. C 48, 2104 (1992).
[14] A. Boudjada, A. Durif, J.Appl.Cryst. 12, 609 (1979).
[15] M. Trojan, D. Brandová, Thermochim. Acta. 161, 11 (1990).
[16] M. Trojan, Thermochim. Acta. 159, 13 (1990).
[17] O. A. Lukyanchenko and V. V. Samuskevich. Thermochim. Acta. 327, 181 (1999).
[18] B. El-Bali, A. Boukhari, R. Glaum, M. Gerk, K. Maaß, Z. Anorg. Allg. Chem. 626, 2557 (2000).
[19] B. Boonchom, S, Youngme, T. Srithanratana, C. Danvirutai. J. Therm. Anal. Calor. 91, 511 (2008).
[20] B. Boonchom, C. Danvirutai. Ind. Eng. Chem. Res. 46,9071 (2007).
[21] M. A.Gabal, Thermochim. Acta. 402, 199 (2003).
[22] L.T.Vlaev, M.M. Nikolova, G.G.Gospodinov. J. Solid State Chem. 177, 2663 (2004).
[23] H.E. Kissinger. Anal. Chem. 29 (1957) 1702.
[24] B.D. Cullity, Elements of X-ray Diffraction, second ed., Addison-Wesley Publishing, (1977).
[25] A.C. Chapman., Apectrochim. Acta. 24A (1968) 1678.
[26] B. Boonchom, C. Danvirutai. J. Optoelect. Adv. Mater. 10, 492 (2008).
[27] M.A.G. Aranda, S. Bruque. Inorg. Chem. 29, 1334 (1990).
[28] M.A.G. Aranda, S. Bruque, J.P. Attfield. Inorg. Chem. 30, 204 (1991)3.
[29] A.G. Nord, T. Stefanidis, Acta Chemica Scandinavica A. 37, 715 (1983).
[30] G. Herzberg, .Molekülspektren und Molekülstruktur. I. Zweiatomige Moleküle., Steinkopff, Dresden (1939).
[31] N.B. Colthup, L.H.Daly, S.E. Wiberley, "Introduction to Infrared and Raman Spectroscopy" Academic Press, New York (1964).
[32] T. Vlase, G. Vlase, M. Doca, N. Doca, J. Therm. Anal. Cal. 72, 597 (2003).

*Corresponding author: kbbanjon@kmitl.ac.th or
bjbchem@yahoo.com (Banjong Boonchom)